Numerical Simulation of a Liquid Jet Impinging on a Moving Substrate

Hatef Rahmani [1], Ali Vakil [1,2], Sheldon I. Green [1]

[1]*Department of Mechanical Engineering, The University of British Columbia - Vancouver*
6250 Applied Science Ln, Vancouver, BC, Canada V6T 1Z4

[2]*Coanda Research and Development Corporation*
6741 Cariboo Rd, Burnaby, BC, Canada, V3N 4A3

Email*: hatef.rahmani@alumni.ubc.ca (H. Rahmani), alivakil@mech.ubc.ca (A. Vakil), Sheldon.Green@ubc.ca*
(S. I. Green)

ABSTRACT

Volume-of-fluid (VOF) CFD simulations are carried out to provide a full description of the lamella characteristics of a Newtonian laminar jet spreading over a smooth moving substrate. The jet Reynolds number and Weber number of the simulations are respectively in the range of 100-2000 and 200-6000. The jet-to-substrate velocity ratio is in the range of 0.1-2.5. The numerical results are validated with data measured on a custom-fabricated spinning disk experimental apparatus. For various combinations of liquid properties, nozzle diameters, and jet-substrate velocities, the lamella dimensions (radius, width and thickness) obtained by simulations agree well with experimental measurements. It is found that at a constant jet diameter and a substrate speed, the lamella thickness scales with the square root of the liquid kinematic viscosity.

Keywords: 3D VOF simulation, jet impingement, jet spreading, lamella dimensions, moving substrate

1. INTRODUCTION

The impingement of high-speed Newtonian and non-Newtonian liquid jets on a moving surface is relevant to a number of industrial processes, including impingement cooling and surface coating. Liquid jet impingement is salient to the railroad industry, where coating of the rail with Liquid Friction Modifiers (LFMs) changes the forces at the wheel-rail interface, resulting in reduced fuel consumption and maintenance costs [1,2].

The impingement of a liquid jet on a flat moving substrate has been studied experimentally for a wide range of liquid properties, surface characteristics, and jet-to-substrate velocities. Keshavarz et al. [3] showed that for low surface and jet speeds the liquid jet spreads laterally from the impingement location forming a lamella, and is then convected downstream, producing an overall U-shaped liquid surface (Figure 1(a)). The U-shape lamella is superficially similar to the Rankine Half body of potential flow, although viscosity plays a key role in determining the lamella geometry. At higher speeds, above a threshold Reynolds number that is a function of the surface roughness, the liquid lamella detaches from the surface, producing jet splash. Keshavarz et al. [3] also reported that the key parameters in determining the outcome of jet impact are fluid viscosity, surface tension, jet and surface speeds. Kumar [4] examined experimentally the effects of viscosity and reported a three-regime splashing-spreading pattern. Moulson, and Green [5] subsequently showed that splash could be suppressed by reducing the surrounding air pressure, thus proving that the air plays a key role in liquid jet splash. Recently, Guo [6] studied the effects of various parameters such as jet and surface speeds and orifice diameter on the lamella geometry. He also made detailed measurements of the dimensions of the liquid surface (Figure 1(b)).

On the numerical side, there have been few attempts to simulate the impingement of a liquid jet onto a substrate and present outcome of the liquid jet after impact, e.g. the free surface characteristics. Gradeck et al. [7] studied the flow fields of a single
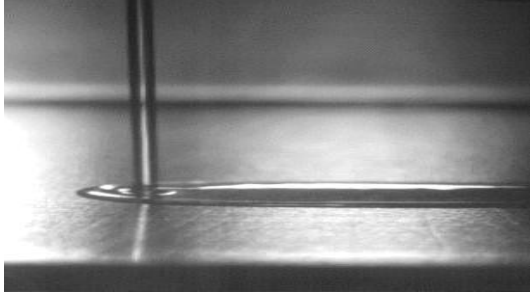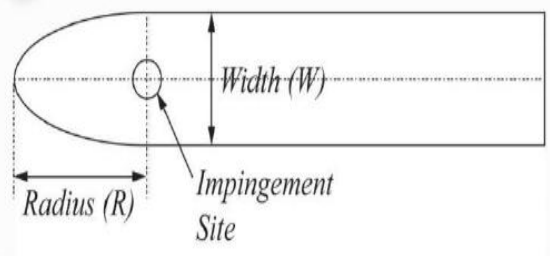
Figure 1: a) Experimental observation of a liquid jet spreading on a moving surface, b) lamella dimensions (top view of jet impingement)

water jet impinging on a moving plate for various jets and nozzle diameters, 17 mm and 20 mm. The numerical predictions of the location and depth of the hydraulic jump for conditions used in rolled metal cooling process were in good agreement with their experimental observations. More recently, Fujimoto et al. [8] examined the flow characteristics of a water jet impinging on a surface covered with a water film. They reported the effects of the jet velocity and nozzle-to-plate distance on detailed flow fields. Later, they extended the simulations to include for multiple circular water jets (Fujimoto [9]). Accordingly, they observed the three modes of flow: stable, unstable, and transient, similar to single jets impinging.

Several researchers studied the liquid jet impingement phenomenon for heat transfer purposes [10-14]. Tong et al. [10] numerically examined the convective heat transfer of liquid jet at around impingement site. They found that the jet velocity had a significant influence on the hydrodynamic development and heat transfer efficiency. Cho et al. [11] carried out numerical study to quantify the liquid surface depth and location for multiple jets in runout table cooling (ROT) processes. They proposed a simple equation to predict the pool height form flow rates, nozzle spacing and pool width. However, most of the works mentioned above are either for low jet and surface velocities or, more importantly, aimed at heat transfer and cooling processes.

The authors know of no previous simulations of high-speed steady laminar jet impingement on a fast moving surface. Thus, the objective of this paper is to present the numerical simulation of the three-dimensional flow field of a liquid jet spreading on a moving substrate. For various jet velocities, substrate velocities, and liquid viscosities, lamella dimensions (radius, width, and thickness) are calculated. Typical

velocity vectors upstream and downstream of the impingement point are presented. The corresponding dimensionless groups for the flow conditions in the current paper are in the following range: $100 < Re_{jet} < 2000, 200 < Re_{sub} < 4500, 200 < We_{jet} < 6000, 5 < V_{jet}(m.s^{-1}) < 25, 10 < V_{sub}(m.s^{-1}) < 60$. The Weber number is presented based on the jet velocity and diameter.

2. NUMERICAL METHOD

In this section the numerical formulations employed to obtain the CFD results are presented. The governing equations are briefly explained. Then, they are followed by the presentation of the computational domain, associated boundary conditions, and the mesh independency check on simulation results.

2.1 Governing Equations

The VOF-based numerical model is used to simulate the steady liquid jet impingement on a moving substrate. The VOF approach solves the conservation of mass and momentum equations for the mixture phase augmented with a continuity equation for the volume fraction of one of the phases to track the interface. The volume fraction for the secondary phase is obtained via the constraint $\alpha_1 + \alpha_2 = 1$. Given the flow is incompressible and the phases are Newtonian, the VOF model takes the following form

$$\frac{\partial \rho}{\partial t} + \vec{\nabla}.\left(\rho\vec{V}\right) = 0 \tag{1}$$

$$\frac{\partial}{\partial t}\left(\rho\vec{V}\right) + \vec{\nabla}.\left(\rho\vec{V}\vec{V}\right)$$
$$= -\vec{\nabla}p + \vec{\nabla}.\bar{\bar{\tau}} + \rho\vec{g} + \vec{F}_{ST} \tag{2}$$

$$\frac{\partial}{\partial t}(\alpha_1) + \vec{\nabla}.\left(\alpha_1\vec{V}\right) = 0 \tag{3}$$

Here α_1 is the volume fraction of the primary phase, ρ and $\vec{V}$ are, respectively, the mixture density and the mixture velocity given by

$$\rho = \alpha_1 \rho_1 + \alpha_2 \rho_2 \qquad (4)$$

$$\rho\vec{V} = \alpha_1 \rho_1 \vec{V}_1 + \alpha_2 \rho_2 \vec{V}_2 \qquad (5)$$

where ρ_1 and ρ_2 are the density of the phases, and $\vec{V}_1$ and $\vec{V}_2$ are the velocity of the phases. The mixture stress tensor is given by

$$\bar{\bar{\tau}} = \mu \left[\vec{\nabla}\vec{V} + \left(\vec{\nabla}\vec{V} \right)^T \right] \qquad (6)$$

with $\mu = \alpha_1 \mu_1 + \alpha_2 \mu_2$ the mixture viscosity; μ_1 and μ_2 are the viscosity of the phases. F_{ST} is the surface tension force incorporated into the momentum equation as a source term via the continuum surface force model proposed by Brackbill et al. [15]. Equilibrium contact angle is considered for all the simulations under the spreading condition.

2.2 Dimensionless Governing Equations

Introducing T as the characteristic time scale, D the characteristic length scale (jet diameter), U the characteristic velocity scale (jet velocity or substrate velocity), and P_0 as the reference pressure, we obtain the following nondimensional variables

$$t^* = \frac{t}{T}, \ \vec{x}^* = \frac{\vec{x}}{D}, \ \vec{V}^* = \frac{\vec{V}}{U}, p^* = \frac{p}{P_0}, \vec{g}^* = \frac{\vec{g}}{g} \qquad (7)$$

The mixture momentum equation renders dimensionless as follows

$$[St]\frac{\partial \vec{V}^*}{\partial t^*} + \vec{\nabla}^*.\left(\vec{V}^*\vec{V}^* \right)$$
$$= -[Eu]\vec{\nabla}^* p^* + \left[\frac{1}{Re} \right] \vec{\nabla}^*. \bar{\bar{\tau}}^* \qquad (8)$$
$$+ \left[\frac{1}{Fr^2} \right] \vec{g}^* + \left[\frac{1}{We} \right] \vec{F}_{ST}^*$$

which contains the following non-dimensional groups

$$St = \frac{D}{TU}, Eu = \frac{P_0}{\rho U^2}, Re = \frac{\rho UD}{\mu}, Fr = \frac{U}{\sqrt{gD}},$$
$$We = \frac{\rho U^2 D}{\sigma} \qquad (9)$$

which are respectively, the Strouhal number, the Euler number, the Reynolds number, the Froude number, and the Weber number.

2.3 Meshing and Boundary Conditions

Figure 2 shows the generic computational domain used for the simulations with the associated boundary conditions. The domain extends from 20D upstream to 80D downstream of the impingement point, where D is the jet diameter. The domain dimensions are given in Figure 2. The lateral walls, considered as the pressure outlet boundary condition, are extended to 40D to assure their impact on the jet flow and spreading physics is insignificant. The typical computational mesh used in the simulations, shown in Figure 3, highlights the small mesh size used in regions of high velocity gradients and around the free surface.
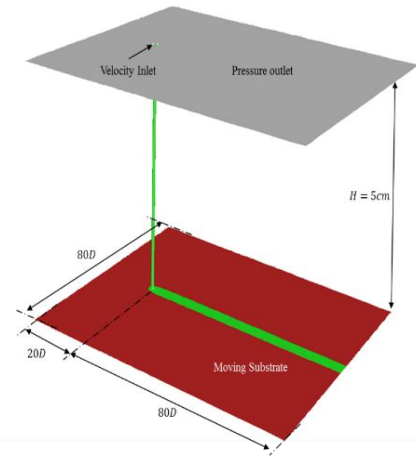
Figure 2: Schematic of the computational domain used for the simulations with the associated boundary conditions (Top); the lateral walls are also considered as the pressure outlet boundary condition.
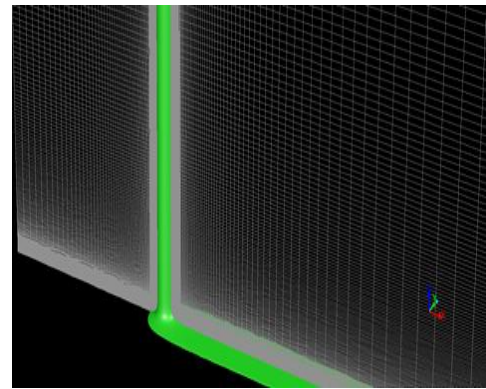
Figure 3: The typical computational mesh used in the simulation

2.4 Mesh Independency Check

To ensure that the obtained data are mesh-independent, several flows were simulated with

different mesh densities. In the refinement procedure, we refined the boundary layer mesh over the moving surface and the structured mesh around the jet free surface. Additionally, we slightly refined the mesh in the outer region of the flow. In general, the lamella thickness (on the order of 50-100 microns) is captured by 3-4 computational cells on the coarse mesh, 5-6 cells on intermediate mesh, and 8-10 cells on the fine mesh. The velocity profiles within the lamella thickness on the symmetry plane at x=1.1D downstream and upstream of the impingement point for different mesh intensities are shown in Figure 4. To estimate the discretization error, we followed the procedure recommended in [16] for the velocity profiles and lamella thicknesses errors. The numerical uncertainty in the fine-grid solution was found to be 4.83% for lamella thicknesses and at most 1.96% for the velocity profiles.

For this particular test, the substrate velocity was 60 m.s^{-1}, the jet velocity was 15 m.s^{-1}, the jet diameter was 650 μm, and the liquid viscosity, density, and surface tension were respectively 40 mPa.s, 1100 kg.m^{-3}, and 0.065 N.m^{-1}. The corresponding jet Reynolds number and Weber number are 268 and 2475.
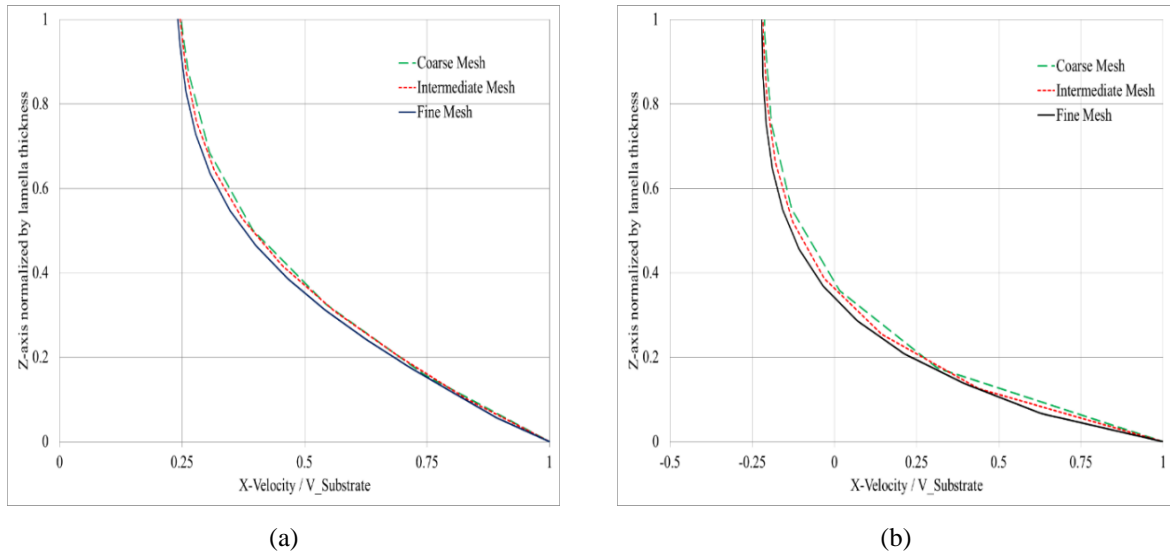
Figure 4: Velocity profile within the lamella for different mesh sizes. (a) Profile extracted along a line normal to the substrate at r=1.1D downstream of the impingement point, (b) Profile extracted normal to the substrate at distance r=1.1D upstream of the impingement point.

2.5 Validation with Experiment

The numerical results are validated with data measured on a custom-fabricated spinning disk experimental apparatus, as shown schematically in Figure 5. Details of the experimental procedure and methodology can be found in Guo and Green [17]. The lamella width and radius from CFD simulations are compared with experimental results in Figure 6(b). The free surface of the liquid was defined to be the location in the flow where the volume fraction is 50%. An interesting result is that the ratio W/R is almost constant, independent of the liquid properties, the jet-substrate speeds, and the jet diameter, as first reported by Guo [6]. The numerical predictions are generally in very good agreement with experimental findings (5.8% rms variance), and almost lie within the error bands of the experiments. However, the agreement between experiments and simulations is less good if one considers separately the values of W and R rather than the ratio of the two; both W and R are slightly over predicted (12.8% on average) by CFD simulations (see Figure 7). The average thickness of the lamella may be inferred from the experimental measurements and application of the continuity equation ($h_{avg} = \frac{Q}{W.V_{sur}}$).
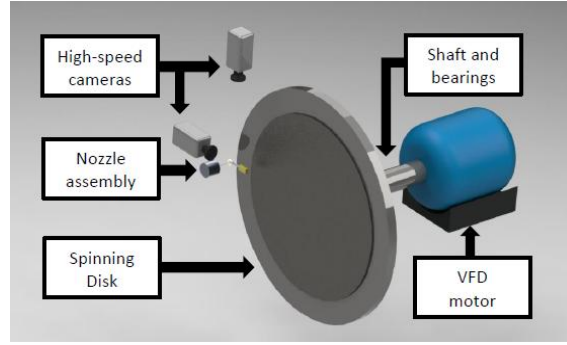
Figure 5: Schematic of experiment apparatus, including spraying system, nozzle assembly, and high speed imaging set-up
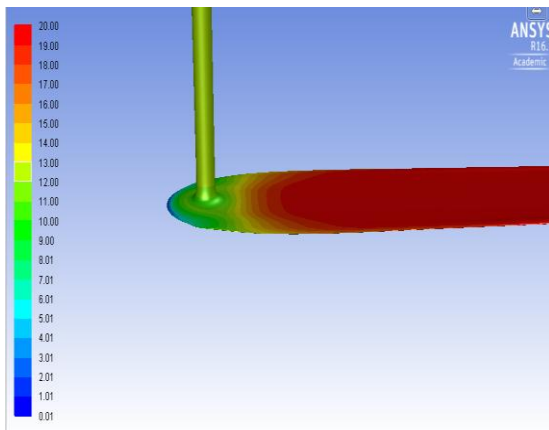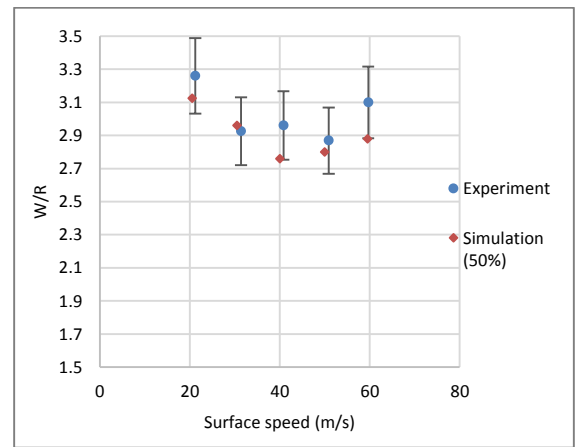
(a)   (b)

Figure 6: a) Free surface from numerical simulation colored by velocity magnitude ($m.s^{-1}$). The substrate is moving from left to right, b) W/R versus surface speed for constant jet velocity of $12\ m.s^{-1}$. The jet diameter is 650 μm, and liquid viscosity, density, and surface tension are respectively 65.3 mPa.s, 1100 kg.m^{-3}, and 0.065 N.m^{-1}. The liquid-air interface is taken to be the surface on which the void fraction is 50%.

3. RESULTS AND DISCUSSIONS

In this section the spreading liquid jet flow fields, including the lamella dimensions and velocity vectors, are presented. Two Reynolds numbers are defined: jet Reynolds number ($Re_{jet} = \rho V_{jet}D/\mu$) and substrate Reynolds number ($Re_{sub} = \rho V_{jet}D/\mu$). The Weber number is also defined based on the jet properties, $We_{jet} = \rho V_{jet}^2 D/\sigma$. In what follows, the impingement point is chosen to be the origin of the coordinate axis. The r-axis is the radial direction and the z-axis is normal to the substrate.

3.1 Lamella Dimensions

Figure 7(a)-(c) respectively show the normalized lamella radius, width, and thickness as a function of

the jet and substrate Reynolds numbers. The lamella thickness is extracted on the symmetry plane at 15D downstream of the impingement point. The simulation revealed that the lamella thickness becomes nearly constant sufficiently far downstream of the impingement location (r>5D for results shown in the figures). This length, where the lamella thickness becomes constant, depends on the liquid properties and the substrate speed. Both W and R are slightly over predicted and h is slightly under predicted by the simulation. However, the simulation results agree well with the experiments, i.e. W and R decrease with substrate speed and increase with jet velocity. The lamella thickness, h, is found to vary inversely with the substrate speed, and vary slightly with the jet velocity.
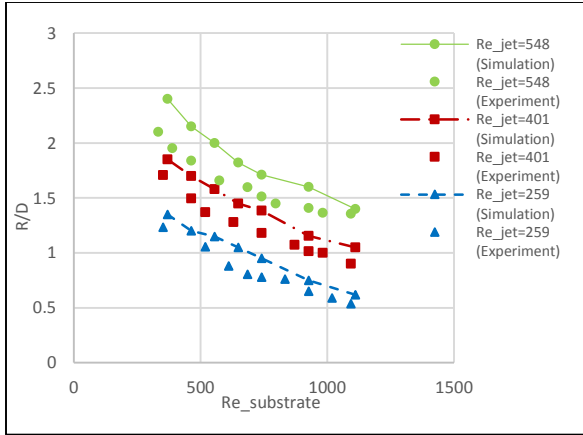
(a) Normalized lamella radius
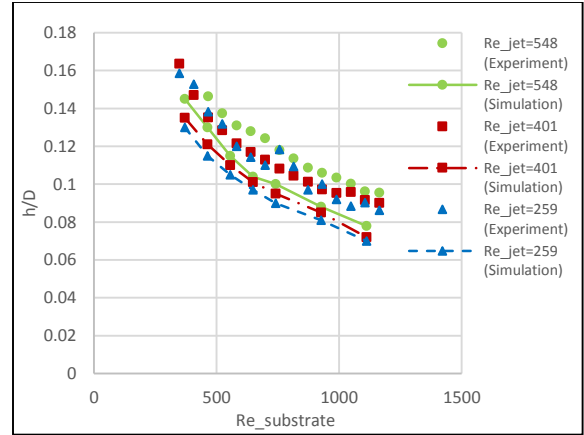
(c) Normalized lamella thickness
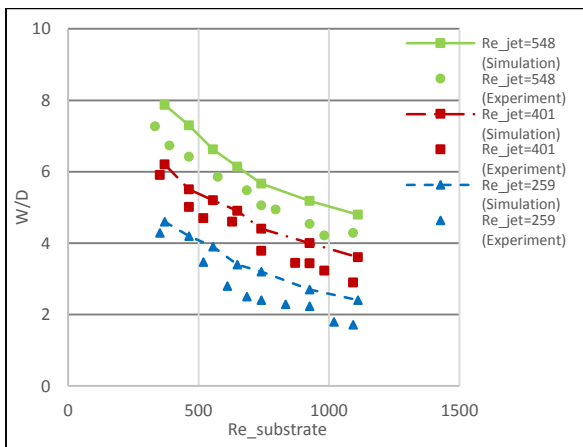
(b) Normalized lamella width

Figure 7: Normalized lamella spread dimensions vs substrate Reynolds number with the jet Reynolds number as a parameter.

Through an order of magnitude analysis of the Navier-Stokes equations in the lamella, Guo [6] found that the average lamella thickness scales with the square root of the liquid kinematic viscosity, similar to the boundary layer thickness in laminar flows. He found experimental validation for this theoretical prediction. Figure 8 shows the average lamella thickness as a function of the square root of the liquid kinematic viscosity for three different substrate speeds (15, 30, 60 $m.s^{-1}$). The jet diameter and velocity are kept constant at 650 μm and 20 $m.s^{-1}$, respectively.
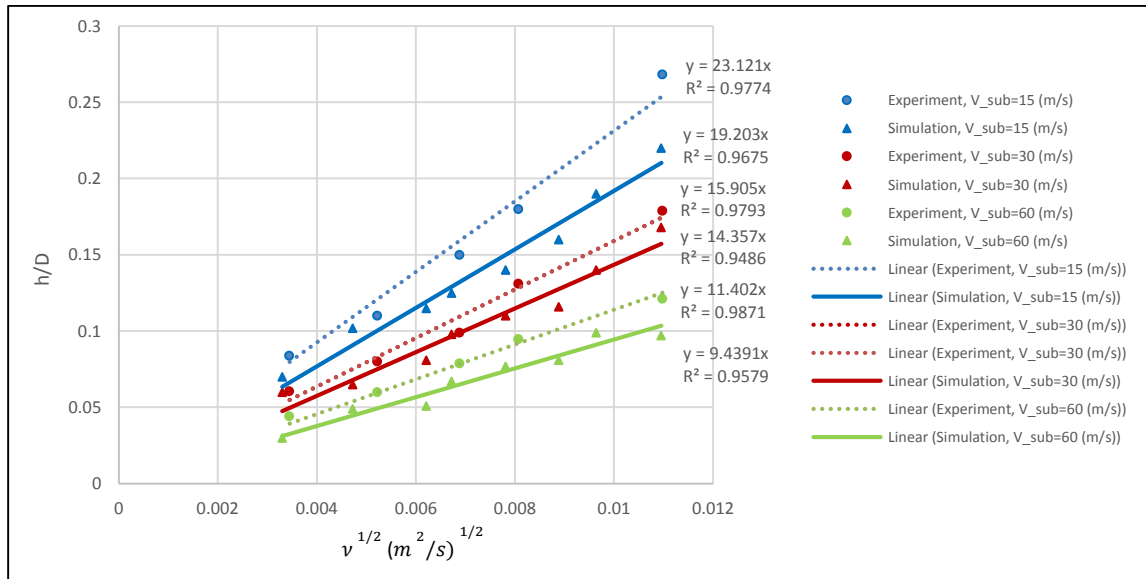
Figure 8: Normalized lamella thickness vs the square root of liquid kinematic viscosity for various substrate speeds

3.2 Velocity Vectors

We present a generic velocity profile of a spreading jet upstream and downstream of the impingement point. Figure 9(a) shows the velocity vectors downstream of the impingement point on the symmetry plane. The vectors are colored by their corresponding phases; red color indicates the liquid phase and the blue color indicates the region filled with air. The lamella thickness gradually decreases as one moves away from the impingement site and becomes nearly constant far enough downstream. Figure 9(b) displays the velocity profiles upstream of the impingement point. The liquid in close proximity to the substrate moves with the substrate speed to the right, while the majority of the lamella thickness moves in the opposite direction with a velocity comparable to the jet velocity. There is a stagnation line along the axis of symmetry of the jet that rises from just above the substrate near the impingement point to near the free surface at the leading edge of the lamella.
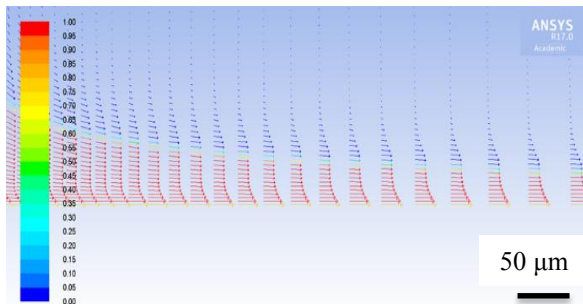
(a) Downstream
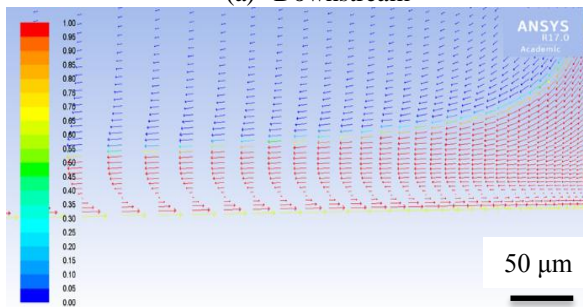
(b) Upstream

Figure 9: Velocity vectors on the symmetry plane, a) downstream, b) upstream. The substrate motion is from left to right at $30\ m.s^{-1}$. The jet velocity, the jet diameter, the liquid viscosity and density are $15\ m.s^{-1}$, 650 μm, 65.3 mPa.s, and 1100 kg.m^{-3}, respectively.

4. CONCLUSIONS

Volume of Fluid CFD simulations of a Newtonian liquid jet spreading over a moving substrate were performed to obtain a full description of the flow field within the lamella thickness. A variety of jet Reynolds number (100-2000), substrate Reynolds number (200-4500), jet Weber number (200-6000), and jet-to-substrate velocity (0.1-2.5) were studied. The numerical results were found to be in good agreement with the experimental measurements. The lamella and typical velocity vectors within the lamella were presented. The key findings of this paper are

- The numerical predictions of the ratio W/R are in very good agreement with the experimental results; both show the ratio remains nearly constant with the substrate speed.
- Both W and R are slightly over predicted by the simulations, while the lamella thickness, h, is slightly under predicted.
- Consistent with previous findings by Guo [6], the lamella thickness varies with the square root of the liquid kinematic viscosity.

ACKNOWLEDGEMENTS

REFERENCES

[1]   J. Cotter, D.T. Eadie, D. Elvidge, N. Hooper, J. Robert, T. Makowsky, Y. Liu. Top of Rail Friction Control: Reductions in Fuel and Greenhouse Gas Emissions. *In: Proc. of the Conference of the International Heavy Haul Association,* 327-334, 2005

[2]   D. T. Eadie, E. Bovey, J. Kalousek. The role of friction control in effective management of the wheel/rail interface. *Railway Technical Conference*, 221-228, 2002

[3]   B. Keshavarz, S.I. Green, M.H. Davy, and D.T. Eadie. Newtonian liquid jet impaction on a high-speed moving surface. *International Journal of Heat and Fluid Flow*, 32(6), 1216-1225, 2011

[4]   P. Kumar. Liquid jet interaction with a moving surface, M.A.Sc. thesis dissertation, UBC, 2012

[5]   J.B.T. Moulson, S.I. Green. Effect of ambient air on liquid jet impingement on a moving substrate. *Physics of Fluids*, 25:102-106, 2013

[6]   Y. Guo. Newtonian and viscoelastic liquid jet impingement on a moving surface. M.A.Sc. thesis dissertation, UBC, 2014

[7]   M. Gradeck, A. Kouachi, A. Dani, D. Arnoult, J. L. Borean. Experimental and numerical study of the hydraulic jump of an impinging jet on a moving surface. *Experimental Thermal and Fluid Science*, 30:193-201, 2006

[8]   H. Fujimoto, Y. Suzuki, T. Hama, H. Takuda. Flow characteristics of circular liquid jet impinging on a moving surface covered with a water film. *ISIJ international*, 51, 1497-1505, 2011

[9]   H. Fujimoto, Y. Lee, R. Kato, T. Hama, H. Takuda. Experimental and numerical study of twin circular water jets impinging on a moving thin film. *ISIJ International*, 2011

[10]   A.Y. Tong. A numerical study on the hydrodynamics and heat transfer of a circular liquid jet impinging onto a substrate, *Numerical Heat Transfer*, 2011

[11]   M.J. Cho, B.G. Thomas, P.J. Lee. Three-dimensional numerical study of impinging water jets in runout table cooling processes. *The Minerals, Metals & Materials Society and ASM International*, 11663-008, 2008

[12]   V.E. Nakoryakov, B.G. Pokusaev, E.N. Troyan. Impingement of an Axisymmetric Liquid Jet on a Barrier. *Int. J. Heat Mass Transfer*, 21:1175-1184, 1978

[13]   Y.A. Buyevich, V. Ustinov. Wydrodynamic conditions of transfer processes through a radial jet spreading over a flat surface. *International Journal of Heat and Mass Transfer,* 37:165-173, 1992

[14]   A.K. Mozumder, Y. Mitsutake, M. Monde. Subcooled water jet quenching phenomena for a high temperature rotating cylinder. *International Journal of Heat and Mass Transfer*, 68:466-478, 2014

[15]   J.U. Brackbill, D.B. Kothe, C. Zemach, A continuum model for modelling surface tension. *Journal of Computational Physics*, 100:335-354, 1992

[16]   P.J. Roache, Quantification of uncertainty in computational fluid dynamics, *Annual Review of Fluid Mechanics*, 29;23-60, 1997

[17]   Y. Guo, S.I. Green. Visualization of high speed liquid jet impaction on a moving urface. *Journal of Visualized Experiments*, 2015